Journal of Materials Chemistry B

Accepted Manuscript

ROYAL SOCIETY OF CHEMISTRY

www.rsc.org/materialsB

Journal Name

RSCPublishing

PAPER

Bi-functional Co-sensitization of Graphene Oxide Sheets and Ir Nanoparticles on P-type Co_3O_4 Nanofibers for Selective Acetone Detection

Cite this: DOI: 10.1039/x0xx00000x

Received 00th January 2012,
Accepted 00th January 2012

DOI: 10.1039/x0xx00000x

www.rsc.org/

Seon-Jin Choi,[a] Won-Hee Ryu,[b] Sang-Joon Kim,[a] Hee-Jin Cho[a] and Il-Doo Kim*[a]

We report on highly sensitive and selective acetone detection achieved by sensitizing p-type Co_3O_4 nanofibers (NFs) with Ir nanoparticles (NPs) and graphene oxide (GO) sheets for potential diagnosis of diabetes. Co_3O_4 NFs mixed with Ir NPs (1 wt%, average particle size 6 nm) were further functionalized by GO sheets (1 wt%) to investigate the dual-sensitization effect on cross sensitivity for acetone, pentane, NO, NH_3, CO and NO_2. These Ir- and GO-co-functionalized Co_3O_4 NF composites exhibited high acetone response (R_{gas}/R_{air}=2.29) at 5 ppm. This value was 58% and 36% greater than that of the pristine Co_3O_4 NFs (R_{gas}/R_{air} =1.45) and Ir-functionalized Co_3O_4 NFs (R_{gas}/R_{air}=1.69), respectively. The detection limit of Ir- and GO-co-functionalized Co_3O_4 NF sensors is predicted to be as low as 120 ppb, presenting the response value of 1.18 at 300 °C. Furthermore, superior acetone selectivity, in competition with interfering gases such as pentane, NO, NH_3, CO and NO_2, was investigated. This work demonstrates that optimized co-sensitization of two catalysts (i.e., Ir NPs and GO sheets) on p-type metal oxide NFs, enables the precise detection of exhaled-breath gases for the diagnosis of diabetes.

1. Introduction

Exhaled breath sensors are getting a lot of attention due to potential for simple and non-invasive diagnostic detection of specific diseases by measuring the concentration of breath biomarker gases. Several studies have reported that there are strong correlations between the exhaled breath biomarkers and physical conditions. For example, acetone, ammonia, pentane, carbon monoxide and nitrogen monoxide are closely related to diabetes,[1] kidney malfunction,[2] heart disease (e.g., myocardial infarction),[3] chronic obstructive pulmonary disease (COPD)[4] and asthma.[5] In general, the concentration of exhaled breath gases of healthy people is significantly lower than those of people with such diseases. For this reason, several gas detection methods have been proposed for the accurate analysis of exhaled breath. Typically, exhaled breath has been analyzed by gas chromatography/mass spectroscopy (GC/MS) or optical spectroscopy. However, these types of analyzing equipment are not suitable for real-time diagnosis due to the difficulty in delivery of the bulky equipment and the complexity of its manipulation. As an alternative breath analysis method, chemiresistive sensors using semiconductor metal oxides (SMOs) are getting much attention due to their great potential for realization of low-cost portable devices. This is expected to be done by miniaturization and real-time detection based on a simple operation principle (i.e., fast resistivity changes in a certain gas ambient). Thus far, n-type SMOs such as SnO_2,[6-9] WO_3[10, 11] and ZnO[12] have been widely studied for the detection of hazardous and explosive gases.[13] In contrast, p-type SMOs such as NiO,[14] CuO[15] and Co_3O_4[16] were less actively studied due to the low gas sensitivity, which limits their broad application in gas sensing research. The poor gas sensing characteristics of p-type SMOs are attributed to low carrier mobility (for example, 0.2 $cm^2/V{\cdot}s$ of p-type NiO compared with 160 $cm^2/V{\cdot}s$ of n-type SnO_2) which hinders fast signal transfer through the sensing electrodes.[17] In addition, it was reported that modulation of the hole accumulation layer in p-type SMOs is relatively less effective compared to modulation of the electron depletion layer in n-type SMOs during gas reactions between the adsorbed oxygen ions (O^-, O^{2-}) and the target gases,[18] which results in the low gas sensitivity of p-type SMOs. Gas sensors using p-type SMOs still hold great potential for selective detection capability, in particular when the p-type SMO is functionalized with an n-type SMO or metallic catalysts.[19, 20] For this reason, combination with n-type material by forming p-n junction structure has been proposed. Examples include SnO_2 nanocrystal functionalized CuO nanowire,[21] Cr_2O_3 functionalized ZnO nanowire[22] and NiO-SnO_2 composite nanofiber[23] to enhance the gas sensing capability of p-type SMOs. In addition, doping with metallic catalysts such as Pt,[24] Au,[25] Cr[19] and Fe[20] was suggested for chemically or electronically sensitizing p-type SMO to enhance the selective properties. More recently, graphene based materials (i.e., graphene, graphite and graphene oxide); which show p-type sensing characteristics, were functionalized on the p-type SMO surface as newly proposed sensing composites. The graphene sheets exhibit high specific surface area (theoretically 2630 m^2/g) and high mobility (200,000 $cm^2/V{\cdot}S$); which can improve the gas sensing characteristics by providing increased surface

reaction sites as well as a fast-carrier transport pathway. For these reasons, graphene oxide (GO)-WO_3,[26] reduced graphene oxide (RGO)-Cu_2O,[27] RGO-SnO_2,[28] graphene sheet-Cu_2O,[29] and RGO-Co_3O_4[30] composite sensing materials were synthesized for the detection of NO_2 and H_2S. Even though efforts were made to enhance the p-type SMO sensing properties, they still showed low sensitivity for precise exhaled breath sensing due to the decreased sensing characteristics of SMO in highly humid atmosphere.[31, 32] Several research groups proposed a dual catalytic effect that might be achieved by co-sensitization of two different catalysts on the SMO. Esfandiar *et al* demonstrated TiO_2 nanoparticles coupled on reduced graphene oxide; followed by decoration of Pt and Pd nanoparticles using the sol-gel method.[33] In addition, Russo *et al* proposed GO coated SnO_2 nanoparticles followed by Pt nanoparticle deposition, using microwave-assisted synthesis.[34] These materials are typical examples using the dual catalytic effect on SMO base materials for the detection of H_2. Enhanced sensing properties were observed in the dual catalyst functionalized SMO due to the enhanced chemical or electronic sensitization by the catalysts. However, those types of co-sensitization have not been widely tried, and most cases were based on n-type SMO layers.

In this work, for the first time, we propose p-type Co_3O_4 exhaled breath sensing materials which are functionalized with Ir nanoparticles (NPs) and graphene oxide (GO) sheets to facilitate the dual catalytic effect. Co_3O_4 NFs were synthesized by electrospinning, which is a facile and versatile method to obtain high surface-to-volume ratio, one-dimensional (1D) nanostructures. Ir NPs with the average particle size distribution of ~6 nm; which were synthesized by polyol method, were decorated on Co_3O_4 NFs and then GO sheets were additionally functionalized on the surface of the Ir-loaded Co_3O_4 NFs. The breath sensing characteristics were evaluated by injecting biomarker gases toward the dual catalysts functionalized Co_3O_4 NF sensors at highly humid atmosphere (90% RH); which is similar to human breath. The main focus of this study was the demonstration of the dual catalytic effect for achieving highly sensitive and selective breath sensing capability of Ir- and GO-functionalized Co_3O_4 NFs; thereby opening up the possibility of application for the diagnosis of diabetes.

2. Experimental Details

2.1 Materials

Cobalt (II) acetate tetrahydrate [$CH_3(COO)_2Co{\cdot}4H_2O$], polyvinylpyrrolidone (PVP, M_w= 1,300,000), *N,N*-dimethylformamide, chloroiridic acid [H_2IrCl_6], ethylene glycol, ethanol, and graphene oxides (GO) were purchased from Sigma-Aldrich (St. Louis, USA). All the chemicals were used without further purification.

2.2 Preparation of Co_3O_4 nanofibers (NFs)

Highly crystallized Co_3O_4 nanofibers (NFs) were prepared by electrospinning and subsequent calcination in air. To prepare the electrospinning solution, 3 g of $(CH_3COO)_2Co{\cdot}4H_2O$ was dissolved in 7.5 g of *N,N*-dimethylformamide and continuously stirred at room temperature for 1 h. Then, 1 g of PVP was dissolved and stirred in the precursor solution for 6 h. Electrospinning was performed with the controlled feeding rate of 0.5 mL h^{-1} and the electrospun Co precursor/PVP composite NFs were collected on stainless steel foil which was vertically positioned 15 cm away from the syringe needle (25 gauge) under a constant potential of 20 kV. The obtained as-spun Co precursor/PVP composite NFs were calcined at 600 °C for 1 h in air atmosphere.

2.3 Synthesis of Ir nanoparticles (NPs)

Ir NPs were synthesized as catalytic materials for the functionalization on the Co_3O_4 NFs. The Ir NPs were prepared by the polyol method as described in the previous work.[10] The detailed experimental procedures are described in the ESI†.

2.4 Characterization

The microstructures and morphologies of pure Co_3O_4 NFs and the Co_3O_4 NF composites functionalized by Ir NPs and GO sheets (hereafter, we denote the composites as Ir-GO-Co_3O_4 NFs) were examined using scanning electron microscopy (SEM, XL-30 SFEG, Philips). The crystal structure of pristine Co_3O_4 NFs, GO-functionalized Co_3O_4 (GO-Co_3O_4) NFs, and Ir-GO-Co_3O_4 NFs composites were analyzed using X-ray diffraction (XRD, D/MAX-RC 12 kW, Rigaku) with CuKα radiation (λ = 1.54 Å). The microstructure of pristine Co_3O_4 NFs and Ir-GO-Co_3O_4 NFs composites were examined by field-emission transmission electron microscopy (FETEM, Tecnai G2 F30 S-Twin, FEI).

2.5. Sensor fabrication and measurements

To characterize the sensing performance, four different sensors (pristine Co_3O_4, GO-Co_3O_4, Ir-Co_3O_4, Ir-GO-Co_3O_4 NFs) were coated onto a sensor electrode, which is pre-patterned on alumina substrate. The pristine Co_3O_4 NFs were coated onto the prepared substrate by the drop coating method. The synthesized Ir NPs with various contents (0.1-1 wt%) were loaded on the Co_3O_4 NFs by mixing Ir NPs dispersed solution and Co_3O_4 NFs dispersed solution to determine the optimized Ir loading amount. Likewise, different amounts of GO (0.1 and 1 wt%) were functionalized on the Co_3O_4 NFs to confirm the optimum GO content. As a result, 1 wt% Ir NPs functionalized Co_3O_4 NFs (1wt% Ir-Co_3O_4 NFs), 1 wt% GO functionalized Co_3O_4 NFs (1wt% GO-Co_3O_4 NFs); and 1 wt% Ir NPs and 1 wt% GO functionalized Co_3O_4 NFs (1wt% Ir-GO-Co_3O_4 NFs); were fabricated. The solutions of catalyst functionalized Co_3O_4 NFs were identically drop coated onto the sensor substrates. The sensing test system was described in our previous report.[11] Briefly, gas sensing characteristics were evaluated by measuring the resistivity change during the cyclic exposure of target gases and air. Considering the breath sensor application, several target gases (i.e., acetone, pentane, nitrogen monoxide, ammonia, carbon monoxide and nitrogen dioxide), known to be disease markers for diabetes, heart disease, asthma, kidney failure and COPD; were selected. The target gas injection time and the stabilization time in air were fixed for 10 min. The gas sensing test was conducted at highly humid atmosphere (90% RH) to maintain the similar environment with the exhaled breath. The resistivity changes were measured using a data acquisition system (34972A, Agilent) with a 16 channel multiplexer (34902A, Agilent). Based on the changes in resistivity measured, gas response (R_{gas}/R_{air}) was evaluated. Here, the R_{air} and R_{gas} denote the resistivity when the sensors were stabilized in air and when the target gas was injected toward the sensors, respectively. The operating temperature of

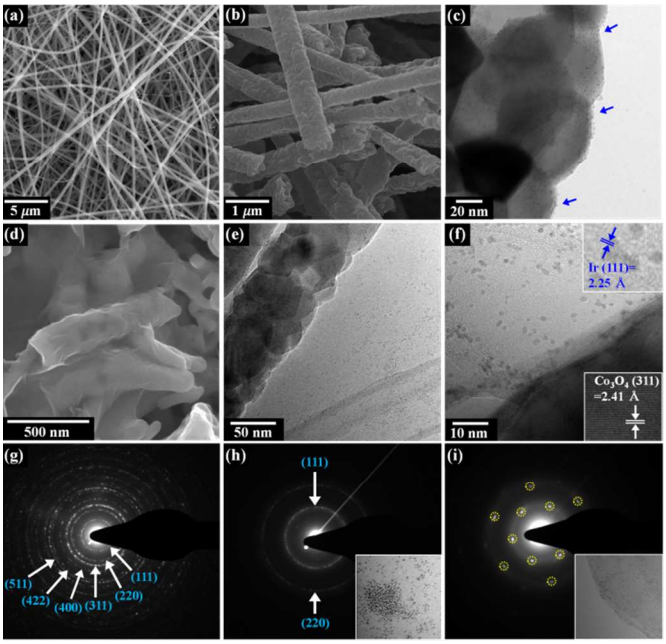

Fig. 1 SEM images of: (a) as-spun Co precursor/PVP NFs and (b) pristine Co_3O_4 NFs after calcined at 600 °C for 1h; (c) TEM image of 1wt% Ir-Co_3O_4 composite NFs; (d) SEM image of 1wt% Ir-GO-Co_3O_4 composite NFs; (e) TEM image of 1wt% Ir-GO-Co_3O_4 NFs; (f) High-resolution TEM (HRTEM) image of 1wt% Ir-GO-Co_3O_4 NFs. Selected area electron diffraction (SAED) patterns of: (g) pristine Co_3O_4 NFs, (h) Ir nanoparticles, and (i) thin layer of GO

the sensors was controlled by applying voltage to the heating electrodes using a DC power supply (E3647A, Agilent). The sensors were stabilized for ~6 h in the baseline gas (humid air) at the operating temperature prior to the gas sensing measurements.

3. Results and Discussion

3.1 Microstructural and chemical analysis

The synthesized Co_3O_4 NFs; as well as composites with Ir NPs and GO, are described in Fig. 1. The prepared as-spun Co precursor/PVP composite fibers showed a non-woven structure with the average diameter of 500–700 nm (Fig. 1a). During the calcination step, the as-spun fibers were shrunk by the decomposition of the PVP polymer domain, and the Co precursor was oxidized to form Co_3O_4. The calcined Co_3O_4 NFs exhibited decreased diameters of approximately 300 nm (Fig. 1b). The synthesized Co_3O_4 NFs were functionalized with Ir NPs, and subsequently GO sheets were functionalized to investigate the dual catalytic effect on gas sensing characteristics. First, Co_3O_4 NFs were functionalized with Ir NPs as shown in Fig. 1c. In the TEM image, several Ir NPs were clearly observed on the surface of the Co_3O_4 NF (blue arrows). Then, GO were functionalized with Ir NPs-Co3O4 NFs composites. The SEM observation revealed that the GO-incorporated Ir NPs-Co_3O_4 NF composites were clearly presented (Fig. 1d). The flexible characteristics of GO enable containing several Ir NPs-Co_3O_4 NF composites. However, the Ir NPs could not be observed using SEM due to the limited capability for detection of such small nanoparticles (~6 nm). TEM analysis, for the detailed structures and morphological observation of the composite sensing materials, was performed. This indicated the pristine Co_3O_4 NFs which exhibited discrete nanorod shapes originated from the broken long NFs. The functionalization of polycrystalline Co_3O_4 NFs with Ir NPs and GO were also confirmed using TEM (Fig. 1e). Ir NPs were clearly observed on the GO sheet; as well as on Co_3O_4 NFs. High resolution TEM (HRTEM) images showed well crystallized Co_3O_4 with the interplanar distance of 2.41 Å. This corresponds to the (311) plane (inset of Fig. 1f at the bottom). In addition, crystalline Ir NP with (111) plane was observed with the interplanar distance of 2.25 Å (inset of Fig. 1f, at the top). Selected area electron diffraction (SAED) patterns were investigated in Fig. 1g-i. Polycrystalline Co_3O_4 NFs were confirmed; with lattice planes of (111), (220), (311), (400), (422) and (511). The polycrystalline characteristic of Co_3O_4 was also confirmed by the noticeable grain boundaries shown in TEM image (Fig. 1e). The Ir NPs synthesized by the polyol process exhibited a crystalline nature with the lattice planes of (111) and (220) (Fig. 1h). Regarding the SAED pattern of GO sheets, a graphene-like hexagonal pattern, which originated from the honeycomb lattice structure of graphitic crystalline, was clearly observed(Fig. 1i).[35] The blurred SAED pattern image indicates that the multi-layered GO sheets were stacked together; and included impurities or functional groups such as oxygen species or local defects.[36]

To confirm the crystalline structure of pristine Co_3O_4 NFs; as well as the Ir-GO-Co_3O_4 NF composites, X-ray diffraction (XRD) analysis was performed (Fig. S1 in the ESI†). As shown in Fig. 2a, pristine Co_3O_4 NFs showed characteristic peaks of planar directions of (111), (220), (311), (222), (400), (422) and (511); which were also confirmed by the SAED pattern in Fig. 1g. However, the characteristic peaks of Ir and GO could not be identified in the composite materials of 1 wt% GO-Co_3O_4 NFs and 1 wt% Ir-GO-Co_3O_4 NFs. This absence of characteristic peaks of Ir and GO was probably because they were present in traces below the XRD detection limits. The existence and the crystal structure of GO were investigated using Raman spectroscopy with a 514 nm laser (Fig. 2). Pristine Co_3O_4 NFs showed only Si substrate characteristic peak at the Raman shift of 521 cm^{-1} without any characteristic peaks of GO sheets (Fig. 2a). When 1 wt% GO sheets were functionalized on the surface of Co_3O_4 NFs, characteristic Raman shifts of GO were observed both for 1 wt % GO-Co_3O_4 NF and for 1 wt% Ir-GO-Co_3O_4 NF samples (Fig. 2b and c). The characteristic peaks of GO were exhibited at the 1594 cm^{-1} for G band, which is generated from the first-order scattering of the E_{2g} mode of sp^2 domains,[37] and 1348 cm^{-1} for D indicating sp^2 destruction due to defect formation.[38] Further confirmation of the existence of Ir and GO were performed by energy-dispersive X-ray spectroscopy (EDX) elemental mapping of the Ir-GO-Co_3O_4 NF composite (Fig. S2 in the ESI†).

The chemical composition and bonding state of the Ir-GO-Co_3O_4 NF composites were examined by X-ray photoelectron spectroscopy (XPS, Sigma Probe, Thermo VG Scientific) (Fig. 3). The XPS spectrum confirmed the existence of four components - Co, Ir, O and C - from the GO sheet, Ir NPs and Co_3O_4 NFs. The high resolution of the XPS spectrum at the Co 2*p* peaks showed two distinct peaks at binding energies of 779.9 eV for $2p_{1/2}$ and 795.2 eV for $2p_{3/2}$, which were generated from Co_3O_4 NFs (Fig. 3a).[39] The composition of the Ir NPs was confirmed that the dominant binding state was IrO_2 indicated by the binding energies of 61.1 eV for $4f_{7/2}$ and64.1 eV for $4f_{5/2}$.[40] Weak peaks at the binding energies of 62 eV and 65 eV, which were generated from the $4f_{7/2}$ and $4f_{5/2}$, respectively, corresponded to metallic Ir. The plotted residual curve

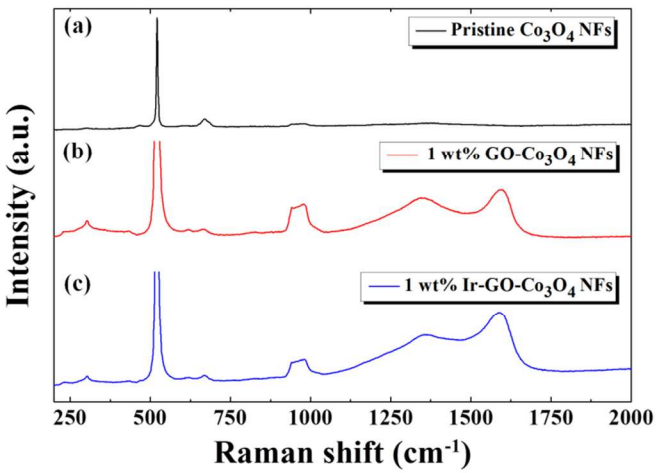

Fig. 2 Raman spectra (514 nm excitation) of: (a) pristine Co_3O_4 NFs, (b) 1 wt% GO-Co_3O_4 NFs and (c) 1 wt% Ir-GO-Co_3O_4 NFs

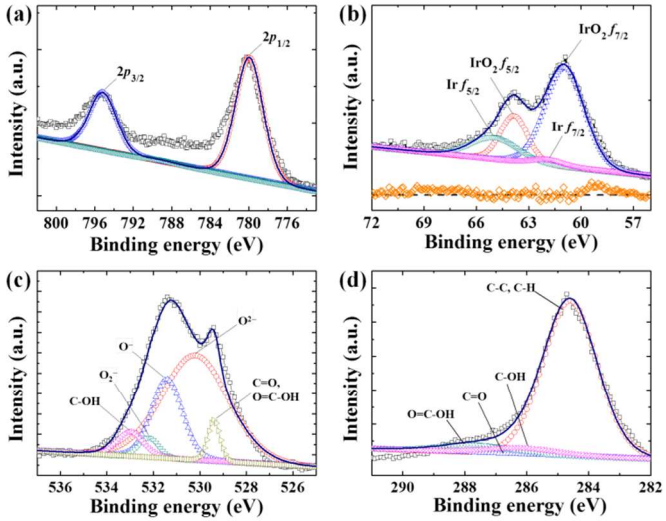

Fig. 3 X-ray photoelectron spectroscopy (XPS) analysis using high resolution spectra in the vicinity of the: (a) Co 2*p*, (b) Ir 4*f*, (c) O 1*s* and (d) C 1*s*.

identified the high quality of the fitting procedure (Fig. 3b). From these results, it was confirmed that Ir NPs were severely oxidized by forming IrO_2 (n-type) near the surface; which can induce p-n junction with the contact of p-type GO and Co_3O_4 NFs. It is assumed that the formation of IrO_2 from Ir NP can occur during the functionalization with Co_3O_4 NFs and GO due to the high surface energy at the nanoscale (~6 nm) particle size.[41] The asymmetric O 1*s* spectrum can be resolved into several peaks that corresponded to O^{2-}, O^- and O_2^- with binding energies of 530.2 eV, 531.4 eV and 532.2 eV, respectively. These characteristic binding energies were assumed to indicate the adsorption of chemisorbed oxygen species at the surface of Co_3O_4 NFs. Additionally, minor peaks at 533 eV and 529.4 eV were attributed to the C-OH and C=O, O=C-OH groups; which probably belonged to the GO sheets (Fig. 3c).[42] The high resolution spectrum of C 1*s* has a main peak in the range of 284.6 eV that corresponds to C=C and C-H bonding, and three minor peaks at 288.9, 287.7 and 286.2 eV that correspond to O=C-OH, C=O and C-OH groups, respectively (Fig. 3d).[42]

3.2 Gas sensing characteristics and discussion

For the potential application in exhaled breath sensors to diagnose of diabetes, acetone sensing characteristics at highly humid ambient (90% RH) were evaluated (Fig. 4). To confirm the optimum composition of Ir NPs and Co_3O_4 NFs, various amounts of Ir NPs (0.1 wt%, 0.5 wt% and 1 wt%) were functionalized on the Co_3O_4 NFs. Analysis of the acetone sensitive characteristics revealed that increased in response (R_{gas}/R_{air}=1.7) at 5 ppm of acetone with an operating temperature of 300 °C, was observed with the sensor of 0.1 wt % Ir NPs functionalized Co_3O_4 NFs; compared to that (R_s=1.45) of pristine Co_3O_4 NFs. However, decreased acetone sensitivities were observed with samples of 0.5 wt% and 1 wt% Ir NPs functionalized Co_3O_4 NPs exhibiting the response values of 1.34 and 1.07 at 5 ppm of acetone, respectively (Fig. 4a). Investigation of the dynamic sensing properties of resistivity transients with respect to time revealed that the baseline resistivity increased with the Ir NP content (Fig. 4b-e), which was attributed to effective formation of p-n junctions between IrO_2 NPs and Co_3O_4 NFs. Interestingly, 1 wt% Ir-Co_3O_4 NFs showed n-type sensing characteristic at 1 ppm of acetone (Fig. 4e), in contrast with pristine Co_3O_4 NFs, 0.1 wt% Ir-Co_3O_4 NFs and 0.5 wt% Ir-Co_3O_4 NFs (Fig. 4b-d) which all exhibited p-type sensing characteristics. The p-n transition of 1 wt% Ir-Co_3O_4 NFs was attributed to n-type IrO_2 formed by the oxidation of Ir at an elevated operating temperature.[10, 43] In addition, thermally excited electrons in the conduction band of Co_3O_4 NFs can probably accelerate the conversion of the major carriers to electrons. The n-type property of 1 wt% Ir-Co_3O_4 NFs can induce chemisorbed oxygen species (O^-, O_2^-) on the surface to form depletion layers, which increase the baseline resistivity. These chemisorbed oxygen species will be released by the injection of acetone, which in turn decreases the baseline resistivity as in the following equation (1).[43, 44]

$$CH_3COCH_3\ (gas) + 8O^-(chemisorbed) \rightarrow 3CO_2 + 3H_2O + 8e^- \quad (1)$$

Even though high acetone sensitivity was observed with the sample of 0.1 wt% Ir-Co_3O_4 NFs, it was assumed that the Ir catalytic effect was dominant when the 1 wt% Ir was functionalized on Co_3O_4 NFs, considering the occurrence of n-p transition during the dynamic acetone sensing. For this reason, GO sheets were functionalized with 1 wt% Ir-Co_3O_4 NFs and compared with the pristine Co_3O_4 NFs, with 1 wt% GO-Co_3O_4 NFs, and with 1 wt% Ir-Co_3O_4 NFs. The optimum GO content on acetone sensing characteristics were also confirmed when the GO sheets were functionalized with Co_3O_4 NFs (Fig. S3 in the ESI†). GO of 1 wt% was chosen for the functionalization with 1 wt% Ir-Co_3O_4 NFs, owing to the slightly increased acetone response (R_{gas}/R_{air}=1.5 at 5 ppm) of 1 wt% GO-Co_3O_4 NFs compared to that (R_{gas}/R_{air}=1.45 at 5 ppm) of the pristine Co_3O_4 NFs. In addition, it was appropriate to maintain the same weight ratio between GO and Ir considering the optimum acetone sensing characteristic of GO/Ir composite sensors (Fig. S4 in the ESI†). Fig. 4f shows acetone response of pristine Co_3O_4 NFs, 1 wt% GO-Co_3O_4 NFs, 1 wt% Ir-Co_3O_4 NFs and 1 wt% Ir-GO-Co_3O_4 NFs with the concentration range of 1–5 ppm at 300 °C. The result revealed that the composite sensing material of 1 wt% Ir-GO-Co_3O_4 NFs showed the highest response, R_{gas}/R_{air} 2.29; which is 58% higher than the response (R_{gas}/R_{air}=1.45) of pristine Co_3O_4 NFs at 5 ppm of acetone. The 1 wt% GO-Co_3O_4 NF showed the second highest response toward acetone with the response of 1.50 at 5 ppm, which is similar to that of pristine Co_3O_4 NFs. Temperature dependent acetone sensing characteristics were investigated in the

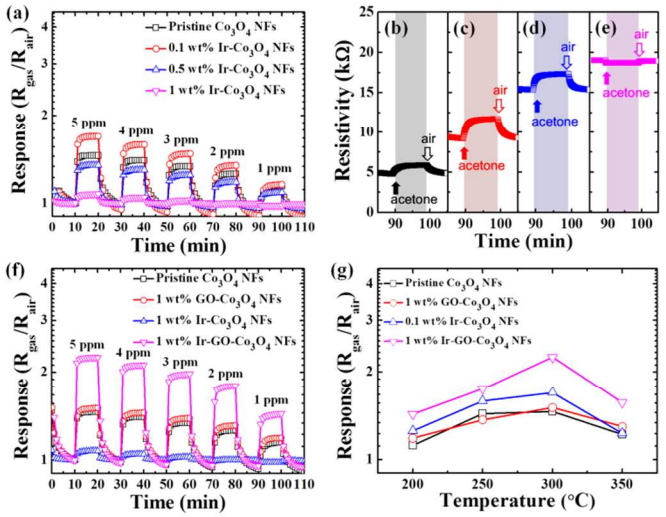

Fig. 4 Response characteristics of pristine Co_3O_4 NFs, 0.1 wt% Ir-Co_3O_4 NFs, 0.5 wt% Ir-Co_3O_4 NFs and 1 wt% Ir-Co_3O_4 NFs toward acetone in a the concentration range of 1–5 ppm at 300 °C (a); Dynamic acetone sensing properties of: (b) pristine Co_3O_4 NFs, (c) 0.1 wt% Ir-Co_3O_4 NFs, (d) 0.5 wt% Ir-Co_3O_4 NFs and (e) 1 wt% Ir-Co_3O_4 NFs at a the concentration of 1 ppm at 300 °C; (f) Dynamic response characteristics with acetone in a concentration range of 1–5 ppm at 300 °C; and (g) temperature dependent response properties in the temperature range of 200–350 °C of pristine Co_3O_4 NFs, 1 wt% GO-Co_3O_4 NFs, 1 wt% Ir-Co_3O_4 NFs and 1 wt% Ir-GO-Co_3O_4 NFs toward 5 ppm acetone

temperature range of 200–300 °C (Fig. 4g). It was demonstrated that all four different sensors showed optimum response at the operating temperature of 300 °C. In addition, 1 wt% Ir-GO-Co_3O_4 NFs exhibited higher response at all operating temperatures. Higher concentrations of Ir/GO were incorporated with Co_3O_4 NFs to confirm the optimized composition. The result revealed that decreasing acetone response characteristics (R_{gas}/R_{air}=1.39, 1.19 and 1.04 at 5 ppm) were observed with increasing Ir/GO concentrations (2 wt%, 5 wt% and 10 wt% Ir-GO-Co_3O_4) at 300 ˚C (Fig. S5 in the ESI†), which demonstrated that 1 wt% Ir-GO-Co_3O_4 NFs exhibited optimal sensing performance (R_{gas}/R_{air}=2.29) at given operating temperature.

To understand the exceptionally improved acetone response with 1 wt% Ir-GO-Co_3O_4 NFs, the sensing mechanism of p-type SMO should be investigated. In principle, p-type SMO sensing materials show resistivity changes in a gas ambient by thinning or thickening the hole-accumulation layer near the surface. This is due to the adsorption and desorption of negative charged oxygen species such as O^- and O_2^-. Unlike n-type SMO sensing materials, p-type sensors show less dependence on morphological configuration. It was reported that square root times low sensitivity can be obtained theoretically with a p-type SMO compared to that of an n-type SMO; with identical structure and morphology.[45] For this reason, morphological modification of p-type SMOs to enhance the gas response is known to be an ineffective approach.[19] Electronic sensitization to control the acceptor/donor density, was proposed as an effective way to maximize the modulation of the hole accumulation layer; thereby improving the sensitivity of p-type SMOs.[19, 46] The electronic sensitization effect can be observed by the increased resistivity due to the reduced hole concentration near the surface. This results from electron-hole recombination. As confirmed in Fig. 4b-e, it was revealed that Ir NP functionalized Co_3O_4 NFs showed increased baseline

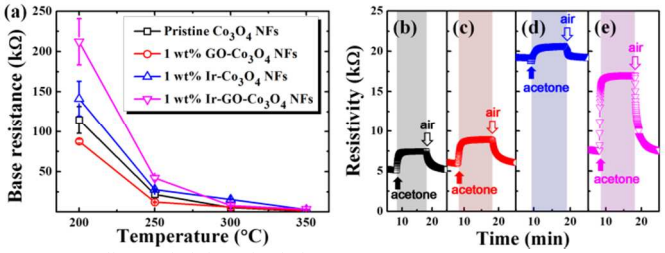

Fig. 5 Baseline resistivity of pristine Co_3O_4 NFs, 1 wt% GO-Co_3O_4 NFs, 1 wt% Ir-Co_3O_4 NFs and 1 wt% Ir-GO-Co_3O_4 NFs with the operating temperature range of 200–350 °C (a); Dynamic resistivity transient with respect to time of: (b) pristine Co_3O_4 NFs, (c) 1 wt% GO-Co_3O_4 NFs, (d) 1 wt% Ir-Co_3O_4 NFs and (e) 1 wt% Ir-GO-Co_3O_4 NFs toward 5 ppm acetone at 300 °C

resistivity; which was attributed to effective electronic sensitization of Ir NPs. In the same way, baseline resistivity of 1 wt% Ir-GO-Co_3O_4 NFs was identified and compared with other composites (Fig. 5). The result showed that dramatically increased baseline resistivity (212 kΩ) was observed with 1 wt % Ir-GO-Co_3O_4 NFs; compared to that of 1 wt% Ir-Co_3O_4 NFs (141 kΩ) and pristine Co_3O_4 NFs (114 kΩ) at 200 °C. This implies the occurrence of electronic sensitization (Fig. 5a). The electronic sensitization in the 1 wt% Ir-GO-Co_3O_4 NFs can occur at both interfaces of Ir/Co_3O_4 NFs and Ir/GO. This resulted in higher baseline resistivity than that of 1 wt% Ir-Co_3O_4 NFs at 200 °C. However, decreased baseline resistivity (88 kΩ) was observed with 1 wt% GO-Co_3O_4 NFs at 300 °C. This was assumed to be because GO behaves like an electron conductor by effectively transferring carriers to the sensing electrodes at elevated operating temperature. The decrease in baseline resistivity with the increase in operating temperature, was attributed an increase in carrier density caused by thermal excitation. The dynamic sensing properties with the resistivity transient was evaluated with 5 ppm acetone at 300 °C to compare resistivity changes and sensing characteristics (Fig. 5b-e). Similar baseline resistivity and resistivity changes during the acetone and air injection were observed with pristine Co_3O_4 NFs (Fig. 5b) and 1 wt% GO-Co_3O_4 NFs (Fig. 5c). In the case of the 1 wt% Ir-Co_3O_4 NFs, (Fig. 5d), a sudden increase in resistivity was observed due to the effective electronic sensitization of the Ir NPs. However, reduced baseline resistivity, as well as highly improved changes in resistivity during exposure to acetone and air, was observed with the 1 wt % Ir-GO-Co_3O_4 NFs (Fig. 5e). The reduced baseline resistivity was attributed to the improvement of carrier transport by the GO functionalization,[41] and the large resistivity change was attributed to the effective electronic sensitization of Ir on both the GO and Co_3O_4 NFs surfaces.

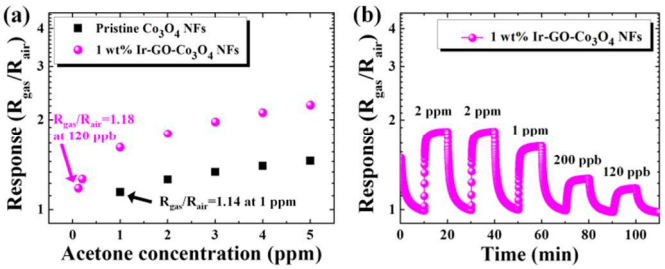

Fig. 6 Limit of detection capability of pristine Co_3O_4 NFs and 1 wt% Ir-GO-Co_3O_4 NFs of acetone in a concentration range of 120 ppb–5 ppm at 300 °C (a); (b) Dynamic response characteristics of 1 wt% Ir-GO-Co_3O_4 NFs toward acetone with a concentration range of 120 ppb–2 ppm at 300 °C

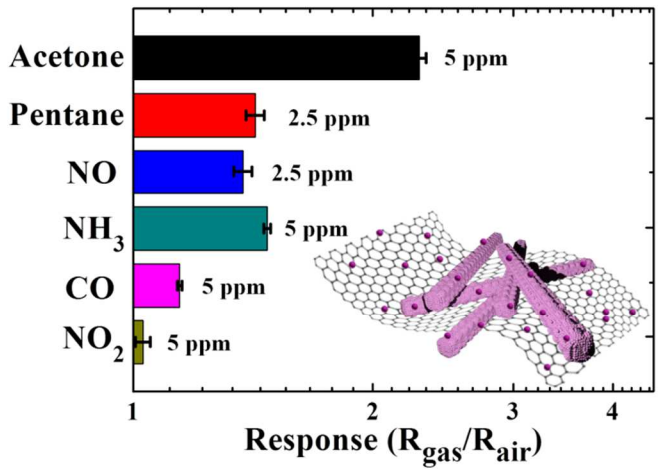

Fig. 7 Selective characteristic of 1 wt% Ir-GO-Co_3O_4 NFs with acetone gas concentration of 2.5–5 ppm and operating temperature at 300 °C

The limit of detection of acetone is an important parameter for the applications aimed at diagnosis of diabetes. It was reported that acetone at concentrations at and above 1.8 ppm is exhaled from diabetes patients. This is 2–6-fold higher than the 300-900 ppb of acetone exhaled by healthy people.[1] As shown in Fig. 6a, the proposed 1 wt% Ir-GO-Co_3O_4 NF sensor showed outstanding acetone detection capability down to 120 ppb with the response of 1.18 at 300 °C. In contrast, the pristine Co_3O_4 NF sensor showed the response of 1.14 at 1 ppm of acetone at the same operating temperature. The dynamic sensitive characteristics of the 1 wt% Ir-GO-Co_3O_4 NF sensor showed stable response and recovery properties during cyclic exposure to acetone and baseline air; at 10 min intervals (Fig. 6b). Based on evaluation of the detection limit, the proposed exhaled breath sensing composite of 1wt% Ir-GO-Co_3O_4 NFs, is extremely promising for use as an exhaled acetone sensing layer, and has the capability to detect acetone at very low concentrations.

The selective detection characteristic is another important parameter for an exhaled breath sensor considering that exhaled breath contains a number of different biomarker gases. Fig. 7 presents the acetone selective characteristics of the 1 wt% Ir-GO-Co_3O_4 NF sensor with respect to other typical biomarker gases such as pentane, NO, NH_3, CO and NO_2 with response values toward each gas at 2.5–5 ppm and operating temperature at 300 °C. The result revealed that the 1 wt% Ir-GO-Co_3O_4 NF sensor showed the highly selective properties (R_{gas}/R_{air}=2.29) toward acetone with minor response (<1.5 of R_{gas}/R_{air}) toward interfering gases. This demonstrated the potential for application of exhaled acetone sensing for the diagnosis of diabetes.

4. CONCLUSIONS

In this work, two different catalyst functionalized p-type Co_3O_4 NFs were synthesized and demonstrated superior acetone sensing characteristics for application as exhaled breath sensors. The Co_3O_4 NFs were synthesized by electrospinning; which is a facile approach to obtain nanofibrous nonwoven structure with a high-surface-to volume ratio. Catalytic materials containing Ir NPs synthesized by the polyol method, and GO, were functionalized with the Co_3O_4 NFs to induce a dual catalytic effect. The sensing characteristics of the composites were demonstrated with acetone gas concentration as low as 120 ppb at highly humid ambient (90% RH). This is a far lower acetone concentration than that in the exhaled breath of healthy people (~900 ppb). The sensing result showed that the highly sensitive characteristics were obtained with 1 wt% Ir-GO-Co_3O_4 NFs (R_{gas}/R_{air} values of 2.29 at the acetone concentration of 5 ppm; at 300 °C). In addition, a very low detection limit with stable sensing capability was confirmed at 120 ppb of acetone with the response of 1.18. This was higher than that of pristine Co_3O_4 (R_{gas}/R_{air}=1.14) NFs at 1 ppm. Furthermore, remarkable acetone selective property was demonstrated; along with minor response toward other typical breath biomarkers such as pentane, NO, NH_3, CO and NO_2. The highly sensitive and selective characteristics of the 1 wt% Ir-GO-Co_3O_4 NFs sensor were attributed to the dual catalytic effect from combining Ir NPs and GO. The Ir NPs induced effective electronic sensitization by thinning the hole accumulation layer on the surface of Co_3O_4 NFs, as well as GO. In addition, the highly conductive GO provided fast carrier transfer to the sensing electrodes, which contributed to improved response. These results revealed that the proposed sensing composite of 1 wt% Ir-GO-Co_3O_4 NFs showed great potential for application in an exhaled breath sensor for detection of trace exhaled acetone; thereby, the rapid, noninvasive diagnosis of diabetes.

Acknowledgements

This work was supported by the Center for Integrated Smart Sensors funded by the Ministry of Science, ICT & Future Planning as Global Frontier Project (CISS-2012M3A6A6054188).

Notes and references

[a]Department of Materials Science and Engineering, Korea Advanced Institute of Science and Technology, Daejeon 305-701, Republic of Korea. E-mail addresses: idkim@kaist.ac.kr; Fax: +82-42-350-3310; Tel.: +82-42-350-3329

[b]Department of Chemical and Environmental Engineering, Yale University, New Haven, Connecticut 06520-8286, United States

†Electronic Supplementary Information (ESI) available: STEM image and energy-dispersive X-ray spectroscopy (EDX) elemental mapping of Ir-GO-Co_3O_4 NFs. Acetone sensing characteristics of GO-Co_3O_4 NF composite sensors. Acetone sensing characteristics of GO-Ir composites, temperature dependent acetone response of Ir-GO-Co_3O_4 NFs with different Ir/GO concentrations. See DOI: 10.1039/b000000x/

1. M. Righettoni, A. Tricoli and S. E. Pratsinis, *Anal. Chem.* 2010, 82, 3581-3587.
2. L. R. Narasimhan, W. Goodman and C. K. N. Patel, *P. Natl. Acad. Sci. U.S.A.*, 2001, 98, 4617-4621.
3. Z. W. Weitz, A. J. Birnbaum, P. A. Sobotka, E. J. Zarling and J. L. Skosey, *Lancet*, 1991, 337, 933-935.
4. P. Paredi, S. A. Kharitonov, D. Leak, S. Ward, D. Cramer and P. J. Barnes, *Am. J. Res. and Crit. Care Med.* 2000, 162, 369-373.
5. E. Tseliou, V. Bessa, G. Hillas, V. Delimpoura, G. Papadaki, C. Roussos, S. Papiris, P. Bakakos and S. Loukides, *Chest*, 2010, 138, 107-113.
6. N. G. Cho, D. J. Yang, M. J. Jin, H. G. Kim, H. L. Tuller and I. D. Kim, *Sens. Actuators, B*, 2011, 160, 1468-1472.
7. I. S. Hwang, J. K. Choi, H. S. Woo, S. J. Kim, S. Y. Jung, T. Y. Seong, I. D. Kim and J. H. Lee, *ACS Appl. Mater. Interfaces* 2011, 3, 3140-3145.
8. B.-H. Jang, O. Landau, S.-J. Choi, J. Shin, A. Rothschild and I.-D. Kim, *Sens. Actuators, B*, 2013, 188, 156-168.
9. J. Shin, S. J. Choi, I. Lee, D. Y. Youn, C. O. Park, J. H. Lee, H. L. Tuller and I. D. Kim, *Adv. Funct. Mater.* 2013, 23, 2357-2367.

10. J. Shin, S. J. Choi, D. Y. Youn and I. D. Kim, *J. Electroceram.* 2012, 29, 106-116.
11. S. J. Choi, I. Lee, B. H. Jang, D. Y. Youn, W. H. Ryu, C. O. Park and I. D. Kim, *Anal. Chem.* 2013, 85, 1792-1796.
12. J. Huang, H. Ren, P. Sun, C. Gu, Y. Sun and J. Liu, *Sens. Actuators, B*, 2013, 188, 249-256.
13. I. D. Kim, A. Rothschild and H. L. Tuller, *Acta Mater*. 2013, 61, 974-1000.
14. N. G. Cho, I. S. Hwang, H. G. Kim, J. H. Lee and I. D. Kim, *Sens. Actuators, B*, 2011, 155, 366-371.
15. S. Steinhauer, E. Brunet, T. Maier, G. C. Mutinati and A. Köck, *Sens. Actuators, B*, 2013, 186, 550-556.
16. Z. Wen, L. P. Zhu, W. M. Mei, Y. G. Li, L. Hu, L. W. Sun, W. T. Wan and Z. Z. Ye, *J. Mater. Chem. A*, 2013, 1, 7511-7518.
17. N. Yamazoe, G. Sakai and K. Shimanoe, *Catal. Sur. Asia*, 2003, 7, 63-75.
18. H. J. Kim, K. I. Choi, K. M. Kim, C. W. Na and J. H. Lee, *Sens. Actuators, B*, 2012, 171, 1029-1037.
19. H. J. Kim, J. W. Yoon, K. I. Choi, H. W. Jang, A. Umar and J. H. Lee, *Nanoscale*, 2013, 5, 7066-7073.
20. J. W. Yoon, H. J. Kim, I. D. Kim and J. H. Lee, *Nanotechnology*, 2013, 24, 444005.
21. M. Mashock, K. H. Yu, S. M. Cui, S. Mao, G. H. Lu and J. H. Chen, *ACS Appl. Mater. & Interfaces*, 2012, 4, 4192-4199.
22. H. S. Woo, C. Na, I. D. Kim and J. H. Lee, *Nanotechnology*, 2012, 23, 245501.
23. L. Liu, Y. Zhang, G. G. Wang, S. C. Li, L. Y. Wang, Y. Han, X. X. Jiang and A. G. Wei, *Sens. Actuators, B*, 2011, 160, 448-454.
24. N. G. Cho, H. S. Woo, J. H. Lee and I. D. Kim, *Chem. Commun.* 2011, 47, 11300-11302.
25. L. L. Wang, Z. Lou, T. Fei and T. Zhang, *Sens. Actuators, B*, 2012, 161, 178-183.
26. S. J. Choi, F. Fuchs, R. Demadrille, B. Grevin, B. H. Jang, S. J. Lee, J. H. Lee, H. L. Tuller and I. D. Kim, *ACS Appl. Mater. & Interfaces*, 2014, 6, 9061-9070.
27. S. Deng, V. Tjoa, H. M. Fan, H. R. Tan, D. C. Sayle, M. Olivo, S. Mhaisalkar, J. Wei and C. H. Sow, *J. Am. Chem. Soc*. 2012, 134, 4905-4917.
28. S. J. Choi, B. H. Jang, S. J. Lee, B. K. Min, A. Rothschild and I. D. Kim, *ACS Appl. Mater. & Interfaces*, 2014, 6, 2587-2596.
29. L. S. Zhou, F. P. Shen, X. K. Tian, D. H. Wang, T. Zhang and W. Chen, *Nanoscale*, 2013, 5, 1564-1569.
30. N. Chen, X. Li, X. Wang, J. Yu, J. Wang, Z. Tang and S. A. Akbar, *Sens. Actuators, B*, 2013, 188, 902-908.
31. A. Tricoli, M. Righettoni and S. E. Pratsinis, *Nanotechnology*, 2009, 20, 315502.
32. H. R. Kim, A. Haensch, I. D. Kim, N. Barsan, U. Weimar and J. H. Lee, *Adv. Funct. Mater.* 2011, 21, 4456-4463.
33. A. Esfandiar, S. Ghasemi, A. Irajizad, O. Akhavan and M. R. Gholami, *Int. J. Hydrogen Energ*. 2012, 37, 15423-15432.
34. P. A. Russo, N. Donato, S. G. Leonardi, S. Baek, D. E. Conte, G. Neri and N. Pinna, *Angew. Chem. Int. Edit.* 2012, 51, 11053-11057.
35. G. Eda and M. Chhowalla, *Adv. Mater.* 2010, 22, 2392-2415.
36. N. A. Kumar, H. Nolan, N. McEvoy, E. Rezvani, R. L. Doyle, M. E. G. Lyons and G. S. Duesberg, *J. Mater. Chem. A*, 2013, 1, 4431-4435.
37. M. A. Pimenta, G. Dresselhaus, M. S. Dresselhaus, L. G. Cancado, A. Jorio and R. Saito, *Phys. Chem. Chem. Phys*. 2007, 9, 1276-1291.
38. W. H. Yuan, B. Q. Li and L. Li, *Appl. Surf. Sci*. 2011, 257, 10183-10187.
39. D. Patil, P. Patil, V. Subramanian, P. A. Joy and H. S. Potdar, *Talanta*, 2010, 81, 37-43.
40. F. D. Kong, S. Zhang, G. P. Yin, Z. B. Wang, C. Y. Du, G. Y. Chen and N. Zhang, *Int. J. Hydrogen Energ*. 2012, 37, 59-67.
41. G. A. Niklasson and R. Karmhag, *Surf. Sci*. 2003, 532, 324-327.
42. D. Yang, A. Velamakanni, G. Bozoklu, S. Park, M. Stoller, R. D. Piner, S. Stankovich, I. Jung, D. A. Field, C. A. Ventrice and R. S. Ruoff, *Carbon*, 2009, 47, 145-152.
43. N. V. Hullavarad and S. S. Hullavarad, *IEEE T. Nanotechnol*. 2010, 9, 625-629.
44. L. P. Qin, J. Q. Xu, X. W. Dong, Q. Y. Pan, Z. X. Cheng, Q. Xiang and F. Li, *Nanotechnology*, 2008, 19, 185705.
45. M. Hubner, C. E. Simion, A. Tomescu-Stanoiu, S. Pokhrel, N. Barsan and U. Weimar, *Sens. Actuators, B*, 2011, 153, 347-353.
46. N. Yamazoe, *Sens. Actuators, B*, 1991, 5, 7-19.

KAIST Korea Advanced Institute of Science and Technology
291 Daehak-ro, Yuseong-gu Daejeon 305-701 Korea | Tel: +82-42-350-3329 | Email: idkim@kaist.ac.kr

Apr. 9, 2014

Dear Managing Editor Liz Dunn

Graphical Abstract (ToC)

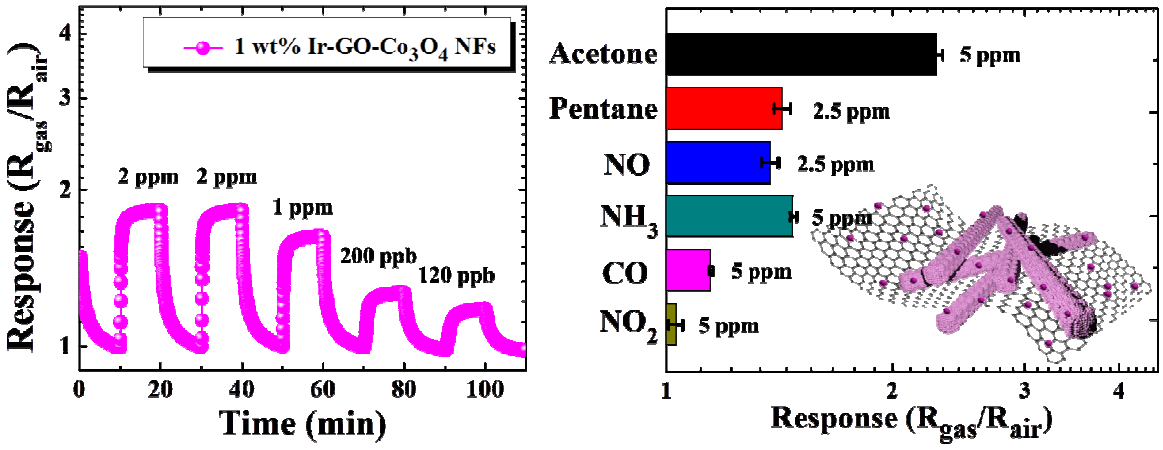

One dimensional p-type Co_3O_4 nanofibers were synthesized by electrospinning which is facile and versatile route to achieve nonwoven structure with high surface-to-volume ratio. Catalytic materials of Ir nanoparticles (NPs) and graphene oxide (GO) sheets were functionalized on the Co_3O_4 nanofibers. Highly sensitive and selective sensing composite were obtained by the dual catalytic effect using Ir NPs and GO sheets, which is promising for the diagnosis of diabetes by detection of exhaled acetone.